The Fracture Process of Toughened Glass

- An Experimental Investigation

Jens H. Nielsen, John F. Olesen & Henrik Stang

Department of Civil Engineering, Technical University of Denmark, DTU†

jhn@byg.dtu.dk jfo@byg.dtu.dk hs@byg.dtu.dk

1 Introduction

The fracture behavior of glass has been studied extensively along with the development of linear elastic fracture mechanics (LEFM) starting in 1920 with the fundamental paper by Griffith[3]. Griffith utilized the mathematical framework for an elliptic crack provided by Inglis[5] and experimentally verified the application of LEFM to glass fracture within 10% accuracy.

The present work is concerned with high-speed observations of the catastrophic fracture propagation in thermally toughened soda-lime-silica glass. The dynamic fragmentation process develops in a fractal manner by repeated branching of propagating cracks. Due to the residual stress state, energy is present at the crack tip at all times, capable of driving cracks into branches; this is observed as a fragmentation process.

2 The Experimental Setup

The specimens used for the present work were all $300\,\mathrm{mm} \times 300\,\mathrm{mm}$ commercially toughened soda-lime-silica glass with various thicknesses ($8\,\mathrm{mm}$, $12\,\mathrm{mm}$ and $19\,\mathrm{mm}$). The fragmentation process was initiated by drilling from the narrow surface into the specimen using a $2.5\,\mathrm{mm}$ diamond drill, water as cooling agent and a setup as indicated in Figure 1.

In order to investigate the characteristic fragmentation of toughened glass, two digital high-speed cameras were used.

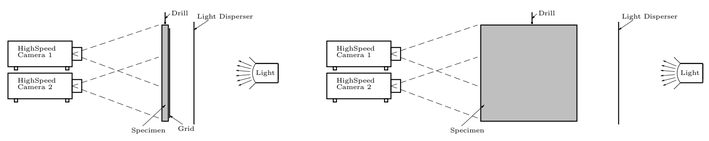

(a) Transverse setup (b) In-plane setup

Figure 1: Sketch of the test setups.

3 Experimental Results

3.1 Crack Propagation Mechanism

Figure 2 shows a series of pictures of the fragmentation process at four different stages; *before fracture*, *initiation of fracture (generation of the Whirl-fragments)*, the *propagation of fragmentation* and the *post fragmentation behavior*.

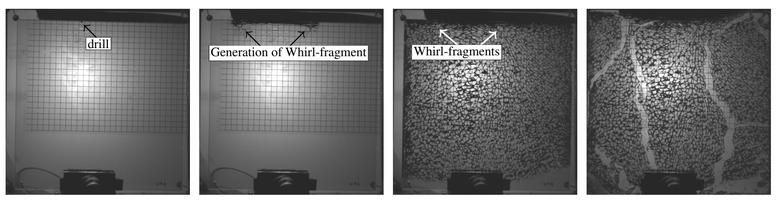

(a) $t = -1.79\,\mu\mathrm{s}$ (b) $t = 0\,\mu\mathrm{s}$ (c) $t = 1.79\,\mu\mathrm{s}$ (d) $t = 13.0\,\mu\mathrm{s}$

Figure 2: Four stages of the fragmentation process

When initiating the fragmentation process in toughened glass, the generation of two larger fragments located adjacently on each side of the initiation point is characteristic [1].

Here, however, fracture initiation from the edge into the center plate plane apparently causes these characteristic fragments to form several centimeters apart, symmetrically about the initiation point. This phenomenon has, to the best of the authors knowledge, never been reported before and will be referred to as formation of the "Whirl-fragments".

The Whirl-fragments are visable from the photo in Figure 3. Two simultaneous fragmentation processes were observed. The origin of a fragmentation process seems to coincide with the initiation of a Whirl-fragment, and it is seemingly located on its boundary at the point most far away from the drill as indicated in Figure 3. Apparently the fragmentation processes are polar as indicated in this figure where the polar coordinates are defined.

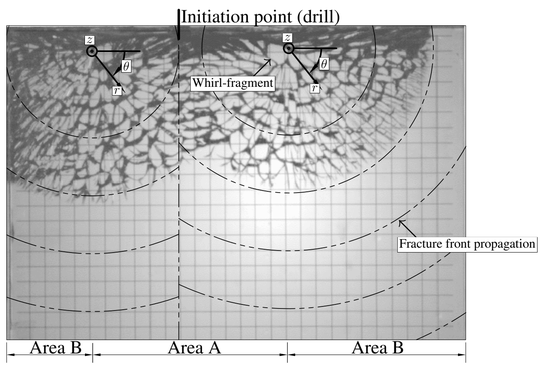

Figure 3: The crack front propagation.

The Whirl-fragments are generated by the branching of cracks. The bifurcation half angles for these branching cracks are approximately $60°$ as shown in Figure 4(h). This is in agreement with the direction for the max principal stress for cracks propagating with velocities above $60\,\%$ of the elastic shear wave speed, as shown by Yoffe[6].

However, [2] states that the attainment of a critical velocity appears to be neither a necessary nor sufficient condition for bifurcation.

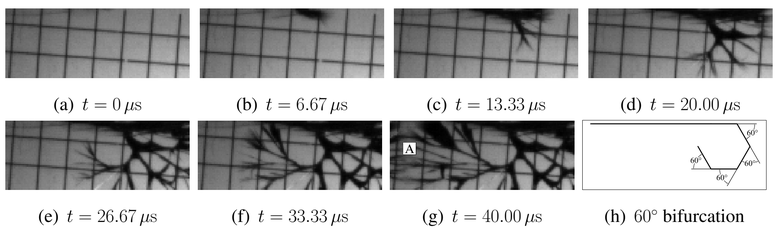

(a) $t = 0\,\mu\mathrm{s}$ (b) $t = 6.67\,\mu\mathrm{s}$ (c) $t = 13.33\,\mu\mathrm{s}$ (d) $t = 20.00\,\mu\mathrm{s}$

(e) $t = 26.67\,\mu\mathrm{s}$ (f) $t = 33.33\,\mu\mathrm{s}$ (g) $t = 40.00\,\mu\mathrm{s}$ (h) $60°$ bifurcation

Figure 4: A close view to the formation of a Whirl-fragment.

3.2 Velocity of the Fracture Propagation Front

Here we have studied 11 specimens, and more than 15 pictures of each specimen were considered to determine the velocity.

Since it is impossible to estimate the location of the apparent center before fracture, it is not possible to make sure that the pictures include this point. Thus, a geometric model was applied, relating the position of the fracture front from the pictures at different times, $u(t)$, to the true velocity. Assuming the true velocity to be constant, and assuming a polar fracture propagation, such a relationship may be derived from geometrical considerations:

$$u(t) = \sqrt{(v(t - t_0))^2 - a^2} - x_0 \tag{1}$$

where v is the true velocity, t is the time, a is the vertical distance from the nearest apparent center to the pictures and x_0 is the vertical distance between the apparent center and $u(0)$, t_0 is a time correction which is fitted along with the true velocity v. Once the constants are estimated, the observations of $u(t)$ can be related to the true velocity v, by a least squares fit of v and t_0.

The fitted values of v and t_0, the goodness of the fit and parameters used for the model can be found in Table 1 for each specimen. Furthermore, the table provides information on the residual stress state in each specimen by giving the average center stresses, $\sigma_{rt,avg}$ and the average stresses at the top surface, $\sigma^{top}_{rc,avg}$.

Table 1: Parameters for equation (1) and measured residual stresses.

Spec.	v	t_0	a	x_0	R^2	$\sigma_{rt,avg}$	$\sigma^{top}_{rc,avg}$
A1	*1472*	*-21.1*	40	0	0.9998	39.6	-69.3
A2	*1451*	*-37*	60	0	0.9989	39.8	-69.3
A3	*1469*	*-27.5*	45	-5	0.9989	36.8	-67.9
A6	*1470*	*-26.4*	50	-10	0.9995	37.2	-68.0
C2	*1471*	*-16*	25	-4	0.9996	45.4	-80.0
C3	*1471*	*-6.5*	20	0	0.9994	46.3	-83.4
C4	*1483*	*-25.6*	42	-3	0.9992	45.9	-81.7
C8	*1452*	*-20.4*	38	-1	0.9996	45.0	-79.6
D1	*1473*	*-1.9*	10	-7	0.9997	50.5	-92.8
D4	*1458*	*-6.9*	18	-5	0.9997	49.4	-92.2
D5	*1460*	*-7.1*	13	-9	0.9998	48.7	-91.1
Avg.	*1466*	*-17.9*	33	-4	0.9995	-	-

A sensitivity analysis of the model parameters was carried out and revealed that the worst combination of parameters changed the velocity by $1.0\,\%$ corresponding to approximately $15\,\mathrm{m/s}$.

3.3 Shape of a Propagating Fracture Front

In Figure 5(a) the drill is clearly visible, however, there is no sign that cracks might have started. In Figure 5(b) the fragmentation has just started, and Figure 5(c) shows the in-plane view of the fracture process generating the Whirl-fragments. Figure 5(d) shows the fracture front at an early stage, and Figure 5(e) and Figure 5(f) show the in-plane shape of the fracture front. Here it is seen that the fracture front propagates almost simultaneously at the surfaces and in the interior, tensile zone.

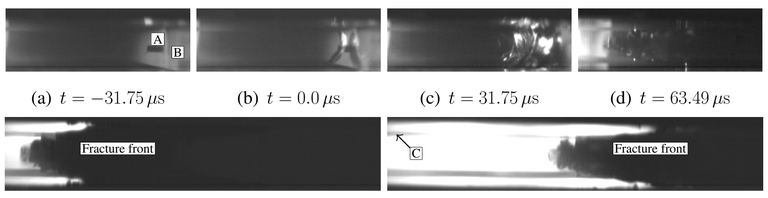

(a) $t = -31.75\,\mu\mathrm{s}$ (b) $t = 0.0\,\mu\mathrm{s}$ (c) $t = 31.75\,\mu\mathrm{s}$ (d) $t = 63.49\,\mu\mathrm{s}$

(e) $t = 95.24\,\mu\mathrm{s}$ (f) $t = 127.0\,\mu\mathrm{s}$

Figure 5: Pictures of the initiation and shape of the in-plane crack front taken with $31\,500\,\mathrm{fps}$ and a shutter time of $1.0\,\mu\mathrm{s}$. A is the drill, B is the narrow surface of the specimen and C is the edge of the narrow side opposite the cameras.

The shape of the fracture front has been sketched in Figure 6(b). For comparison the shape proposed by Acloque [1], based on a post crack investigation is shown in Figure 6(a).

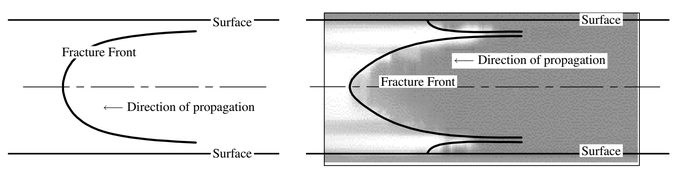

(a) Shape suggested by [1] (b) Shape - High speed observation

Figure 6: Sketches of the in-plane shape of the crack front.

3.4 Post Fracture Investigation

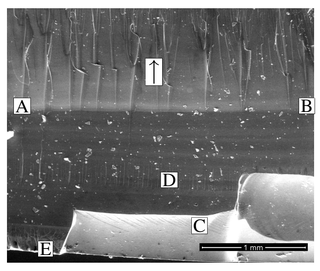

Figure 7: SEM image of fracture surface in a (z,r)-plane, Near the edge.

Figure 7 shows a SEM image of the Hackle zone where the edge of the fracture surface is seen near the bottom of the image, marked with E. A radical change in the topography is marked with A and B. Above this boundary, a hackle topography is seen indicating a fracture propagation direction marked by the arrow, see e.g. [4]. The observations of the fracture propagation are supported by the in-plane shape of the crack front as described earlier and sketched in Figure 6(b).

The area below the boundary A-B is more smooth indicating a lower velocity and a lower energy release rate according to [4]. However, in order to keep pace with the primary fracture propagation, this secondary fracture towards the center plane, must accelerate. Furthermore, small scratches perpendicular to the edge are observed near D. The bright area C is due to large irregularities in the fracture surface caused by chips which have spalled off, and is not interpreted as a fractographic observation.

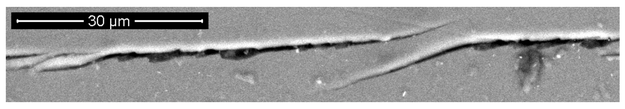

Figure 8: SEM image of a crack on the surface in the (r,θ)-plane of a fractured specimen.

In Figure 8 a SEM image of the regular surface of a fragment with a secondary crack is shown. From the image, it is obvious that there exist crack bridging effects on the micro scale which are partly responsible for keeping the fragments together in large pieces after fracture, as seen in Figure 2(d).

4 Conclusion

The fragmentation was observed to propagate along the edge on both sides of the initiation point for several centimeters before entering into the bulk material, producing two characteristic larger fragments. These two characteristic fragments formed regardless of the specimen thickness; they have not been reported before and are referred to as the *Whirl-fragments* of the fragmentation pattern. It was found that the generation of the Whirl-fragments is caused by the initiation of fracture on the narrow surface at the edge and not by the process of drilling.

From the two Whirl-fragments formed in each specimen, it was found that the origins of the polar crack front propagation were always located on the boundary of the Whirl-fragments at the point most far away from the drill. Hence, it was observed that two distinct polar fracture propagation processes practically developed simultaneously.

The velocity of the fracture propagation front was determined for 11 specimens, using more than 15 pictures of each specimen. The velocity was found to be constant throughout the specimen and it was determined by a least squares fit to the measured data. An average velocity of the fracture front was found to be $1466\,\mathrm{m/s}$ and no correlation was found, neither with respect to thickness nor to the residual stress state. However, it should be noted that a weak correlation between the velocity and the residual stress state has been reported by other authors. A sensitivity analysis on the velocity reveals that it has been determined within an accuracy of $1\,\%$. The in-plane shape of the fracture front was captured, and pictures reveal that the shape derived by only analyzing the so-called Wallner lines is dubious. Pictures showing the in-plane shape of the fracture front have been presented and the local development has been described. SEM images of the fracture surfaces were provided and analyzed, revealing that fractures close to the surfaces were directed towards the center plane of the specimen. Furthermore, a SEM image showing micro-scale crack bridging on the original surface was presented and assumed to be partly responsible for the cohesion between fragments after fracture.

Acknowledgements

The authors would like to thank Mads Bonde at ScanGlas (DK) for providing the glass specimens, The Villum Kann Rasmussen foundation for sponsoring the digital high-speed cameras, and Ebba Cederberg Schnell at DTU-Byg for assisting with the SEM images.

References

[1] P. Acloque. High speed cinematographic study of the fracture process in toughened glass. In *Symposium on Mechanical Strength of Glass and Ways of Improving it*, pages 851–886, 1962. in french.

[2] L. B. Freund. *Dynamic fracture mechanics*. Cambridge University Press, 1990.

[3] A.A. Griffith. The phenomena of rupture and flow in solids. *Philosophical Transactions of the Royal Society of London*, 221:163–198, 1920.

[4] Derek Hull. *Fractography - Observing, Measuring and Interpreting Fracture Surface Topography*. Cambridge University press, 1999.

[5] C. E. Inglis. Stresses in a plate due to the presence of cracks and sharp corners. In *Proc. Inst. Naval Architects*, 1913.

[6] E.H. Yoffe. The moving griffith crack. *Philosophical Magazine*, 42:739–750, 1951.

†Contact information: Technical University of Denmark, Department of Civil Engineering (Att. Jens H. Nielsen), Brovej, Building 118, 2800 Kgs. Lyngby, Denmark

Journal paper submitted to *Experimental Mechanics*